ASSESSMENT OF GLOBAL CLOUD DATASETS FROM SATELLITES:

Project and Database initiated by the GEWEX Radiation Panel

C .J. Stubenrauch[1], W. B. Rossow[2], S. Kinne[3], S. Ackerman[4], G. Cesana[1], H. Chepfer[1], B. Getzewich[11], L. Di Girolamo[5], A. Guignard[1], A. Heidinger[6], B. Maddux[4], P. Menzel[6], P. Minnis[7], C. Pearl[2], S. Platnick[8], C. Poulsen[9], J. Riedi[10], S. Sun-Mack[11], A. Walther[4], D. Winker[7], S. Zeng[10], G. Zhao[5]

1 Laboratoire de Météorologie Dynamique / IPSL / CNRS, Ecole Polytechnique, France

2 CREST Institute at City College of New York, USA

3 Max Planck Institute for Meteorology, Hamburg, Germany

4 CIMMS, University of Wisconsin, Madison, WI, USA

5 Department of Atmospheric Sciences, University of Illinois, Urbana, IL, USA

6 NOAA/NESDIS/STAR, Madison, WI, USA

7 NASA Langley Research Center, Hampton, VA, USA

8 NASA Goddard Space Flight Center, Greenbelt, MD, USA

9 Rutherford Appleton Laboratory, Chilton, UK

10 Laboratoire d'Optique Atmosphérique / CNRS, Lille, France

11 Science Systems and Applications, Inc., Hampton, VA, USA

Corresponding author:

Dr Claudia Stubenrauch

Laboratoire de Météorologie Dynamique

Ecole Polytechnique

F-91128 Palaiseau cedex

France

Phone: +33 169335196

stubenrauch@lmd.polytechnique.fr

ABSTRACT

Clouds cover about 70% of the Earth's surface and play a dominant role in the energy and water cycle of our planet. Only satellite observations provide a continuous survey of the state of the atmosphere over the whole globe and across the wide range of spatial and temporal scales that comprise weather and climate variability. Satellite cloud data records now exceed more than 25 years in length. However, climatologies compiled from different satellite datasets can exhibit systematic biases. Questions therefore arise as to the accuracy and limitations of the various sensors. The Global Energy and Water cycle Experiment (GEWEX) Cloud Assessment, initiated in 2005 by the GEWEX Radiation Panel, provided the first coordinated intercomparison of publically available, standard global cloud products (gridded, monthly statistics) retrieved from measurements of multi-spectral imagers (some with multi-angle view and polarization capabilities), IR sounders and lidar. Cloud properties under study include cloud amount, cloud height (in terms of pressure, temperature or altitude), cloud radiative properties (optical depth or emissivity), cloud thermodynamic phase and bulk microphysical properties (effective particle size and water path). Differences in average cloud properties, especially in the amount of high-level clouds, are mostly explained by the inherent instrument measurement capability for detecting and/or identifying optically thin cirrus, especially when overlying low-level clouds. The study of long-term variations with these datasets requires consideration of many factors. A monthly, gridded database, in common format, facilitates further assessments, climate studies and the evaluation of climate models.

Capsule :

Cloud properties derived from space observations are immensely valuable for climate studies and model evaluation; this assessment has revealed how their statistics may be affected by instrument capabilities and/or retrieval methods but also highlight those well determined.

INTRODUCTION

The GEWEX Radiation Panel (GRP, now the GEWEX Data and Assessment Panel) initiated the GEWEX Cloud Assessment in 2005 to compare available, global, long-term cloud data products with International Satellite Cloud Climatology Project (ISCCP, Rossow and Schiffer 1999), which is the GEWEX cloud product available since the 1980's. The ISCCP cloud products were designed to characterize essential cloud properties and their variation on all key time scales to elucidate cloud dynamical processes and cloud radiative effects. The focus of the assessment is on the comparison of global climatological averages as well as their regional, seasonal and inter-annual variations derived from Level-3 (L3) cloud products (gridded monthly statistics). The presentations and discussions during four international workshops led to the current GEWEX Cloud Assessment database, including monthly averages, a measure of synoptic variability as well as histograms at a spatial resolution of 1° latitude x 1° longitude. It was created in a common netCDF format by the participating teams and is available at the GEWEX Cloud Assessment website: http://climserv.ipsl.polytechnique.fr/gewexca/, together with a detailed report (Stubenrauch *et al.* 2012).

This article presents a summary of average satellite cloud properties and their variability. The GEWEX Cloud Assessment database includes cloud properties retrieved from different satellite sensor measurements, taken at various local times and over various time periods (Tables 1 and 2). Table 3 summarizes the main characteristics of the cloud property retrievals (including spectral domain, spatial resolution, retrieval method as well as ancillary data used) leading to the twelve datasets that participated in the GEWEX Cloud Assessment (Table 1).

SATELLITE REMOTE SENSING OF CLOUD PROPERTIES

Only satellite observations are capable of providing a continuous synoptic survey of the state of the atmosphere over the whole globe. Operational weather satellite sensors have supplied data records extending for over 30 years. Whereas polar-orbiting, cross-track scanning sensors generally only provide global coverage at a particular local time of the day, geostationary satellites are placed at particular longitudes along the equator and permit higher frequency temporal sampling (15 minute to 3 hour intervals).

The relevant passive satellite sensors measure radiation scattered or emitted by the Earth's surface and by the Earth's atmosphere including clouds. To maximize the sensitivity to the presence of clouds and to determine key cloud properties, specific spectral domains are selected. The conversion of the measured radiances into cloud properties requires, in general, two steps:

- cloud detection (or scene identification),
- cloud property retrieval, based on forward model radiative transfer calculations and employing ancillary data to isolate the cloud from surface and non-cloud atmospheric contributions.

Clouds generally appear brighter and colder than the Earth's surface. Cloudy scenes also generally exhibit larger spatial and temporal variability than cloud-free or so called clear sky scenes. However, difficulties in detecting clouds may arise when the radiance contrast is small (e.g. clouds over highly solar reflecting surfaces such as snow or ice, clouds with small thermal contrast to the surface below as for low-level clouds in humid boundary layers over ocean, or cloud edges) or when clear-sky scene variability is larger than usual (e.g. optically thin clouds over heterogeneous land areas or clouds over winter land areas).

Sensor types for retrieving cloud properties

Multi-spectral imagers are radiometers measuring in a limited number of discrete bands, usually from the solar to thermal infrared spectrum. Nadir viewing with cross-track scanning

capabilities, they have a spatial resolution from about 0.5 to 7 km (at nadir) and are the only type of imaging sensors aboard geostationary weather satellites as well as aboard operational polar orbiting satellites. ISCCP uses a combination of these sensors from both, geostationary and polar orbiting satellites to resolve the diurnal cycle of clouds. The commonly available spectral bands are visible and near-infrared (VIS/NIR, day only) and infrared (IR) atmospheric window radiance measurements. Multi-spectral imagers aboard polar orbiting satellites are the Advanced Very High Resolution Radiometer (AVHRR, with 5 spectral channels) aboard the National Oceanic and Atmospheric Administration (NOAA) satellites and the MODerate resolution Imaging Spectroradiometer (MODIS with 36 spectral channels) aboard the National Aeronautics and Space Administration (NASA) Earth Observation System (EOS) satellites Terra and Aqua. Measurements of the same scene under different viewing angles allow a *stereoscopic retrieval of cloud top height*. Together with the use of *polarization* the *cloud thermodynamic phase* can be determined (since non-spherical ice particles polarize the scattered light differently than liquid spherical droplets). The Multi-angle Imaging SpectroRadiometer (MISR, with 4 solar spectral channels and 9 views) aboard Terra and a sensor using POLarization and Directionality of the Earth's Reflectances (POLDER, with 8 solar sub-spectral channels - including 3 polarized - and up to 16 views) aboard PARASOL, being part of the A-Train, both operate during daylight conditions. Results from the Along Track Scanning Radiometer (ATSR, with 7 channels exploring solar to thermal infrared spectrum and 2 views) aboard the European Space Agency (ESA) platforms ERS-2 and Envisat are also provided only for daylight, but a stereoscopic retrieval has not yet been developed.

IR sounders, originally designed for the retrieval of atmospheric temperature and humidity profiles, use IR channels in absorption bands of CO_2, water vapor and ozone. Measured radiances near the centre of the CO_2 absorption band are only sensitive to the upper

atmosphere while radiances from the wing of the band arise from successively lower levels in the atmosphere. The operational High resolution Infrared Radiation Sounder (HIRS, with 19 channels in the IR) is a multi-channel radiometer, whereas the Atmospheric Infrared Sounder (AIRS) and Infrared Atmospheric Sounding Interferometer (IASI) are newer infrared spectrometers. Their spatial resolution is about 15 km (at nadir). Several MODIS channels are similar to those of HIRS, allowing for a similar analysis as for HIRS but with higher spatial resolution. The *variable atmospheric opacity of the many channels measured* by these IR sounding instruments allows a *more reliable identification of cirrus* (semi-transparent ice clouds), *day and night*. Sounder systems usually include **microwave sounders** (Microwave Sounding Unit, MSU, and Advanced Microwave Sounding Unit, AMSU) as well. Because the latter operate at wavelengths insensitive to clouds (sensitive to precipitation, however), they are also used in the retrieval of atmospheric profiles and may be used to improve *cloud detection* (by predicting IR clear sky radiances).

Solar occultation limb sounders, such as the spectrometer of the Stratospheric Aerosol Gas Experiment (SAGE) that measures occultation along the Earth's limb at 4 solar wavelengths, provide *good vertical resolution* (1 km) at the expense of a low horizontal resolution along the viewing path (only about 200 km). On the other hand, the *long atmospheric pathlength* permits the detection of *subvisible (optically very thin) cirrus* (Wang *et al.* 2001).

Passive microwave imagers, like the Special Sensor Microwave Imager (SSM/I) and the Advanced Microwave Sounding Radiometer-EOS (AMSR-E), have frequencies that are sensitive to cloud liquid water (and water vapor) as well as scattering by precipitation-sized ice particles. They may be used to estimate *cloud liquid water path over ocean,* if precipitation and drizzle contamination are removed.

Active sensors extend the measurements of passive radiometers to cloud vertical profiles.

Since 2006 the CALIPSO lidar and CloudSat radar, together, determine cloud top and base heights of all cloud layers (Stephens *et al.* 2002). Whereas the *lidar* is *highly sensitive* and can even detect *sub-visible cirrus*, its beam only reaches cloud base for clouds with an optical depth less than 3. When the optical depth is larger, the radar is still capable of providing a cloud base location. However, the radar signal needs an optical depth greater than about 1.5 to detect a cloud. Even though the nadir-pointing, active instruments have poor global sampling, the *synergy with the passive instruments* participating in the A-Train satellite formation (MODIS, AIRS and POLDER) can be used to better study the v*ertical structure of different cloud types*.

Description of datasets

To resolve the diurnal cycle of clouds the GEWEX cloud climate record, **ISCCP**, emphasizes temporal resolution (eight observations per day), rather than spectral resolution. To achieve this goal with uniform global coverage, the only possibility is to use VIS (day only) and IR atmospheric window radiance measurements from imagers on the suite of geostationary and polar orbiting weather satellites. For a more consistent comparison with the other datasets in the assessment, ISCCP has provided L3 data at four specific local observation times 3:00 AM, 9:00 AM, 3:00 PM and 9:00 PM (the original product is available eight times per day). Cloud pressure (CP) is obtained from the IR radiances and cloud optical depth (COD) is obtained from the VIS radiances, assuming an average effective cloud particle radius (CRE). CRE (and a revised COD, not included here) are retrieved from AVHRR measurements by using shortwave-infrared (SWIR, around 4 μm) spectral information.

The Pathfinder Atmospheres Extended (**PATMOS-x**) was developed by NOAA to take full advantage of all five channels of the AVHRR sensor aboard the NOAA and European Organisation for the Exploitation of Meteorological Satellites (EUMETSAT) polar orbiting platforms. Cloud detection is based on Bayesian classifiers derived from CALIPSO

(Heidinger *et al.* 2010), and the retrieval is based on the Optimal Estimation Method (Heidinger and Pavolonis 2009). First CP and cloud emissivity (CEM) are obtained using two IR channels, then COD and CRE are obtained from solar channels so that finally cloud water path (CWP) can be derived from COD and CRE.

The **ATSR-GRAPE** cloud products (CP, COD, CRE) are retrieved only during day, also using an Optimal Estimation (OE) approach on the five available VIS/NIR/IR channels (Poulsen *et al.* 2010). CWP is derived from COD and CRE.

IR Sounder data have been analyzed to obtain CP and CEM by using two approaches: the 'CO_2 slicing' (**HIRS-NOAA,** Wylie *et al.* 1994, 2006), which is used at lower atmospheric pressures up to 650 hPa and is complemented by the use of an IR atmospheric window radiance, and a weighted χ^2 method using the same CO_2 absorbing channels (**TOVS Path B** and **AIRS-LMD**, Stubenrauch *et al.* 1999, 2006, 2010). The latter datasets also include CREI and CIWP for cirrus, the retrieval based on a Look-Up Table (LUT) approach and spectral emissivity differences between 8 and 12 μm (Rädel *et al.* 203, Guignard *et al.* 2012).

MODIS cloud properties are retrieved by two teams. The MODIS Science Team (**MODIS-ST**) uses 'CO_2 slicing' to determine CP and CEM (Menzel *et al.* 2008) and a LUT approach using solar reflectance channels to retrieve COD and CRE (Platnick *et al.* 2003). The MODIS CERES Science Team (**MODIS-CE**) uses IR radiances to determine CT and CEM, and during the day a reflectance-based LUT approach to retrieve COD and CRE.

POLDER determines cloud thermodynamical phase (Gouloub *et al.* 2000) and COD using VIS/NIR polarization and a LUT approach. CP is determined through differential absorption using 2 channels in the O_2 A-band (Ferlay *et al.* 2010).

MISR provides a stereoscopic cloud top height (CZ) from multi-spectral and multi-angular VIS/NIR measurements (Di Girolamo *et al.* 2010).

The active lidar measurements of the CALIPSO mission are also analyzed by two teams:

the CALIPSO Science Team (**CALIPSO-ST**) determines cloud top height from VIS backscatter and identifies cloud ice from depolarization (Winker *et al.* 2009). Noise is reduced by horizontal averaging. The GCM-Oriented CALIPSO Cloud Products (**CALIPSO-GOCCP**) reduce noise by vertical averaging (Chepfer *et al.* 2010).

Detailed retrieval descriptions may be found in the references of Table 1 and in the GEWEX Cloud Assessment report (Annex I in Stubenrauch *et al.* 2012).

CLOUD AMOUNT

Cloud amount (CA), often referred to as cloud cover or cloud fraction, is the ratio between the number of samples that contain clouds and the total number measurement samples. How instrument resolution (footprint size) affects the estimate of cloud amount has already been studied by Wielicki and Parker (1992), Rossow *et al.* (1993), Maddux et al. (2010): one would expect an *increase in CA by decreasing the spatial resolution* (with the same detection sensitivity), especially in the case of low-level clouds which can be broken and more variable at smaller scales than upper-level clouds. However, the *total cloud amount* determined by a particular instrument also *depends on the sensitivity of its measurements to the presence of clouds.*

- Global total cloud amount (Figure 1) is about 0.68 (±0.03) when considering only clouds with optical depth > 0.1. This value increases to about 0.73 when including sub-visible cirrus (CALIPSO-ST) and decreases to about 0.56 for clouds with optical depth > 2 (POLDER).
- The average global inter-annual variability in CA is about 0.03, about ten times smaller than the typical day-to-day variability over the globe.
- According to most datasets there is about 0.10 to 0.15 more cloudiness over ocean than over land.

Only HIRS-NOAA and MISR detect a ocean-land difference of 0.30, which can be attributed to lowered sensitivity for cloud detection over land (HIRS misses low-level clouds and MISR misses thin cirrus) and to diurnal sampling bias for MISR, which samples only morning conditions (+0.07: due to slightly larger CA over ocean and significantly smaller CA over land in the morning compared to the afternoon).

- The latitudinal variation in CA (Figure 2, upper left panel) of all datasets agrees well (except for polar regions and HIRS-NOAA in Northern Hemisphere (NH) midlatitudes), indicating subtropical subsidence regions with about 0.10 and 0.15 less cloudiness than the global mean at around 20S and 20S respectively and the storm regions in the Southern Hemisphere (SH) midlatitudes with 0.15 to 0.25 more cloudiness than the global mean at around 60S.

This behavior is also shown by the geographical map of regional variations of CA with respect to the global annual mean (0.66), as determined by ISCCP.

Derived cloud amounts depend on instrument capabilities and retrieval performance. To illustrate the spread due to differing sensor sensitivities and retrieval methodologies, Figure 2 presents geographical maps of local differences between maximum and minimum CA value of six datasets (ISCCP, PATMOS-x, MODIS-ST, MODIS-CE, AIRS-LMD and TOVS Path-B), both in a relative and in an absolute sense. The six datasets have been chosen after eliminating datasets taking data at different observation times (MISR and ATSR-GRAPE) and two outliers (HIRS-NOAA, with low sensitivity to low-level clouds, and POLDER, providing information for clouds with optical depth > 2 (Zeng *et al.* 2011)). The CALIPSO datasets were eliminated because of their large sampling noise at 1° latitude x 1° longitude. The global spread in CA of these six datasets corresponds to only 0.08 (Figure 1). However, locally, uncertainties in detecting clouds within the datasets may reach 0.4 over deserts and mountains. Another feature is the InterTropical Convergence Zone (ITCZ) where different

sensitivities to thin cirrus lead to a spread of about 0.15 in CA. The subtraction of the global annual means of the considered datasets leads to slightly improved uncertainty patterns in CA, emphasizing the good agreement for latitudinal variation.

- Most datasets also agree on the magnitude of the seasonal cycle.

In general, the seasonal variations are smaller than the latitudinal variations, except for the transition of the ITCZ towards the summer hemisphere, which produces a change of about 0.30 over land in the latitude band 0°-30S. Over ocean in the NH midlatitudes the seasonal change is about 0.15, with a minimum of cloudiness in late summer, whereas in the SH midlatitudes, it is negligible.

CLOUD TOP LOCATION

Cloud top location can be retrieved in terms of cloud top temperature (CT), pressure (CP) or height (CZ) above mean sea level. For the conversion among these variables one uses atmospheric profiles, which are either retrieved (e.g. for ISCCP, TOVS Path-B and AIRS-LMD) or adopted from reanalyses (e.g. from National Centers for Environmental Prediction (NCEP) for PATMOS-x, MODIS-ST and HIRS-NOAA, European Centre for Medium-Range Weather Forecasts (ECMWF) for ATSR-GRAPE) or taken from weather forecast (e.g. from Global Modeling and Assimilation Office (GMAO) for MODIS-CE and CALIPSO). Differences in monthly statistics can also arise because of differing detection sensitivity to thin, high clouds.

In general, *passive remote sensing provides cloud properties as observed from above.* Therefore high-level clouds correspond to all high-level cloud situations, including single and multiple cloud layers, whereas mid-level and low-level clouds correspond only to situations with no higher altitude clouds above.

Cloud top height (CZ) can be accurately determined with lidar (e.g. CALIPSO).

Apart from the MISR stereoscopic height retrieval for optically thicker clouds, passive remote sensing provides a 'radiometric height', lying near the middle between cloud top and 'apparent' cloud base (for optically thick clouds height at which the cloud reaches an optical depth of 3). It may lie as much as a few kilometers below the 'physical height' of the cloud top, depending on the cloud extinction profile and vertical extent (*cf.* Liao *et al.* 1995, Wang *et al.* 1999, Sherwood *et al.* 2004, Holz *et al.* 2008, Stubenrauch *et al.* 2010). High-level clouds in the tropics generally have such 'diffusive' cloud tops (meaning that the optical depth increases only slowly from cloud top downwards) for which retrieved cloud temperature may be as much as 10 K larger than the cloud top temperature corresponding to a lidar height (Figure 3).

Most sensors with only atmospheric IR window channels retrieve cloud top temperature (CT) assuming that clouds act as blackbody emitters (especially low-level clouds). For semi-transparent clouds the retrieved cloud temperature is therefore biased high because of atmospheric and surface radiation passing through these clouds and needs to be corrected. This can be done by using information on the cloud VIS optical depth or IR emissivity. In the case of multiple cloud layers this correction will be underestimated (*cf.* Jin and Rossow 1997).

Methods involving differential measurements in strong absorption bands (CO_2 or O_2) determine cloud pressure (CP). Whereas the sounding of the thermal CO_2 absorption band leads to a CP corresponding to the radiometric top, the use of the solar O_2 absorption band corresponds to the middle of the cloud (Ferlay *et al,* 2010).

Probability density functions (PDFs) of CP and CT are computed by dividing the histograms available in the cloud assessment database by the number of cloudy samples. Thus they reflect how the detected clouds are vertically distributed in the atmosphere. The PDFs in Figure 3 show a *bimodal structure*, especially in the tropics. This is the reason why *average values of CP and CT may be ambiguous* and why it is *better to use, in addition to averages*

over all clouds, height-stratified averages (intervals for height stratification by CP are indicated in Figure 3).

The *decrease of bimodality and spread in CP and CT from tropics towards poles*, shown by all datasets except HIRS-NOAA, is essentially linked to the *decrease of the tropopause height and a change in the type of atmospheric storm from convective to baroclinic cyclone.* The strong bimodality in the tropics, which is well represented by MODIS-ST, AIRS-LMD, HIRS-NOAA and PATMOS-x with strong peaks at 950 hPa and between 250 and 150 hPa, also means that the tropics have few mid-level clouds, in agreement with local observations using ground-based radar (Mace and Benson-Troth 2002). CP distributions of POLDER and ISCCP are flatter, presenting a larger contribution of mid-level clouds.

CALIPSO is the only mission providing accurate height for cloud top, even for optically very thin clouds such as sub-visible cirrus. Therefore the 'radiative' cloud height retrieved by passive remote sensing should lie below the CALIPSO cloud height. This applies especially to high-level clouds with diffusive tops, which are frequently found in the tropics. In addition, the amplitude of the peak maximum should be smaller because of missed sub-visible cirrus. These criteria are fulfilled by most of the datasets. The peak of ISCCP at very low temperature is explained by the fact that the ISCCP retrieval sets the cloud height to just above the tropopause for optically thin cirrus. A very sharp peak of PATMOS-x in the tropics at 215 K/150 hPa seems to be suspect and can be probably explained by the fact that the PATMOS-x retrieval had been trained by CALIPSO data. Note that when CALIPSO and CloudSat observations are combined a more complete view of cloud vertical structure is obtained (Mace *et al.* 2009).

HEIGHT-STRATIFIED CLOUD AMOUNT

Height-stratified cloud amount relative to total cloud amount gives another indication how

the detected clouds are vertically distributed in the atmosphere. It is less influenced by differences in cloud detection sensitivity and should also be more useful for comparison with climate models, which tend to under-represent the optically thinner clouds.

The global average fraction of high-level clouds out of all detected clouds varies from 12% to 55% (CAHR, Figure 1). This *spread* is essentially *explained by instrument performance to detect and/or identify thin cirrus, especially when overlying low-level clouds (about 20% of all cloudy situations according to CALIPSO-ST data)*: *Active lidar measurements, IR sounding along the CO_2 absorption band and methods using IR spectral differences are powerful for thin cirrus identification (with descending sensitivity from the former to the latter).* Solar reflectance information (during daytime) is more important for the detection of low-level clouds. Thus *the use of different spectral domains is identified as the main reason for discrepancies in retrieved cloud properties, and these can be understood as cloud scene dependent uncertainties and biases.* For cases when thin cirrus is overlying low-level clouds, different retrievals provide different answers: Active lidar and IR methods determine the cloud properties of the thin cirrus (CALIPSO-ST, CALIPSO-GOCCP, HIRS-NOAA, TOVS Path-B, AIRS-LMD, MODIS-ST, MODIS-CE, PATMOS-x), IR–VIS methods (ISCCP, ATSR-GRAPE) provide the properties corresponding to a 'radiative' mean from both clouds while VIS-only methods emphasize the clouds underneath (MISR, POLDER).

- About 40 – 50% of all clouds are high-level clouds. The value decreases to 20% when considering clouds with optical depth > 2 (MISR).

Outliers are HIRS-NOAA (55%, underestimation of low-level clouds leads to overestimation of fraction of high-level clouds) and POLDER (12%, misidentification of high-level clouds as midlevel clouds, because CP determined by O_2 absorption corresponds to a deeper level within the cloud).

- Only about 15% (±5%) of all clouds correspond to mid-level clouds with no higher clouds

above (CAMR, Figure 1).

Values of POLDER (43%), ATSR-GRAPE (39%) and ISCCP (27%) for mid-level cloud amounts are biased high, because of misidentification of high-level clouds overlying lower-level clouds.

- According to the majority of datasets, about 40% (±3%) of all clouds are single-layer low-level clouds (CALR, Figure 1).

Outliers are HIRS-NOAA with 26% (only one IR channel is not sufficient to identify all low-level clouds) and MODIS-ST with 53% (due to misidentification of optically thin cirrus, Holz *et al.* 2008).

By using solar reflectances alone, MISR determines also the height of the low-level cloud when thin cirrus is present above, leading to a relative low-level cloud amount of about 60%, in agreement with 57% from CALIPSO-GOCCP when not only the uppermost clouds are considered but all cloud layers within the atmosphere. This means that about one third of the coverage of all low-level clouds is overlapped by semi-transparent higher-level clouds (also found by studying the frequency of semi-transparent cirrus overlying clouds at lower levels of CALIPSO-ST, *cf.* Jin and Rossow 1997). The merged CALIPSO-CloudSat study by Mace et al. (2009) provides more definitive statistics of multilayer clouds.

- Whereas absolute values of height-stratified cloud amount depend on instrument sensitivity, geographical distributions and latitudinal variations (Figure 2) as well as seasonal cycles of all datasets show very similar features.

Exceptions are polar regions (CAHR in SH and CALR in NH) and CALR of HIRS-NOAA. The geographical maps of the difference between maximum and minimum value of the regional variation as well as of the absolute value of CAHR and CALR out of the six chosen participating cloud datasets (as for CA, see above), also presented in Figure 2, show the spread of CAHR and CALR due to different sensor sensitivity and retrieval methodology.

Whereas the global spread in CAHR and CALR of these datasets correspond to about 0.2 (Figure 1), local spreads of CAHR and CALR may reach even 0.4 (ITCZ and deserts). However, considering variations instead of absolute values (by subtracting global annual means of the considered datasets) leads to spreads mostly less than 0.2 (slightly smaller for CAHR than for CALR).

RADIATIVE CLOUD PROPERTIES

Cloud emissivity (CEM) is retrieved at thermal wavelengths, and values lie between 0 and 1. Its global average is about 0.7 (varying from 0.6 to 0.8). **Effective cloud amount** (CAE, cloud amount weighted by cloud emissivity) includes the radiative effect of the detected clouds. Its global average is about 0.50.

- The global effective amount of high-level clouds (0.15) agrees much better between the different datasets than CAHR, because a smaller cloud amount due to missing thin clouds is compensated by a larger average cloud emissivity (Figure 1).

CLOUD OPTICAL AND BULK MICROPHYSICAL PROPERTIES

Since cloud liquid droplets and ice crystals have different optical properties (linked to refractive index, particle shape and size), it is necessary to distinguish the **cloud thermodynamic phase** before retrieving cloud optical depth and bulk microphysical properties. Liquid and ice clouds are distinguished by polarization measurements (POLDER, CALIPSO), by cloud temperature (ISCCP: ice clouds CT < 260 K, AIRS-LMD, TOVS Path-B: pure ice clouds CT < 230 K, excluding mixed phase clouds) or by use of multi-spectral information (PATMOS-x, MODIS and ATSR-GRAPE). As shown in Figure 4, the global average fraction of ice clouds relative to all clouds (CAIR) lies between 20% (corresponding to pure ice clouds colder than 230 K, without considering mixed phase clouds, thus likely an

underestimate), and 70% (lidar backscatter depolarization), with values around 35% when spectral variation methods are used. Average cloud temperature of definite ice clouds (colder than 230 K) is about 220 K. When warmer ice clouds and possibly mixed-phase clouds are included in the ice cloud category (all datasets except TOVS Path-B and AIRS-LMD), the average ice cloud temperature is about 250 K (Figure 4).

Cloud optical depth (COD) is usually retrieved from a non-absorbing solar reflectance channel (0.5 – 0.9 μm) and therefore only available during daytime, but higher time resolution results from geostationary observations do suggest systematic diurnal variations (Rossow and Schiffer 1999). Given the strong non-linear relationship between reflectance and COD, the most accurate COD values lie between 2 and 50. Whereas **cloud water path** (CWP) strongly influences COD and CEM, **cloud effective particle radius** (CRE, averaged over a size distribution within the cloud) can be obtained from spectral dependency in absorption and scattering in the solar or thermal domain, especially when particles are smaller. At constant CWP, decreasing CRE results in a larger solar albedo. Optical methods determine CRE for all cloud types. However, in the case of optically thick clouds CRE only relates to the upper part of the cloud. This may introduce CRE biases (typically, overestimates for liquid clouds and underestimates for ice clouds). Other sources of uncertainty are assumed particle shape and size distribution within the cloud. Height contributions of CRE depend on the absorbing spectral band used in the retrieval (Platnick 2000); in general, absorption increases with increasing wavelength into the short- and mid-wave infrared (Platnick *et al.* 2003). IR Sounders provide estimates of CRE only for semi-transparent cirrus. CWP can be estimated from COD if CRE is known. Whereas the standard ISCCP product assumes values for CRE in its retrieval of COD (the values of CRE included here for ISCCP come from a special analysis of AVHRR data), other methods retrieve CRE and COD simultaneously, the latter method providing a better estimate.

Global COD varies between 4 and 10 (Figure 4). For comparison, CEM determined by IR sounders was converted to COD which is then limited to values ≤ 10, leading to smaller COD average CODs. Retrieval filtering by MODIS-ST to exclude partly clouds pixels in broken low cloud regions results in larger mean COD compared to other datasets (Zhang and Platnick 2011; Pincus et al. 2012); in addition, COD is truncated to 100 when COD > 100 resulting in a low mean bias for the thickest convective cloud regions relative to other dataset that have a higher truncation limit. For ATSR-GRAPE, the OE retrieval method successful only for about 40% of all clouds, with a bias towards optically thick clouds) leads to larger averages for these products (Figure 5). Given a global mean cloud amount of nearly 0.70, the radiative mean cloud COD has to be < 4 to give a planetary albedo near 0.3.

Since PDFs of COD are not Gaussian (Figure 5) and averages depend on pixel-level filtering choices before/after the retrieval, it is strongly recommended that the distributions be considered instead of averages. One can distinguish three groups in Figure 5: clouds with COD < 1, with COD between 1 and 10 and with COD > 10. The main contribution to global averages comes from clouds with COD between 1 and 10 (except ATSR-GRAPE), and the relative contributions outside this range essentially reflect *differences in data selection for the retrieval.*

- Global effective particle radii are about 14 μm (±1 μm) and 25 μm (±2 μm), for the tops of liquid clouds and for high-level ice clouds respectively (Figure 4).
- Effective cloud droplet radii (CREW) are on average about 15 – 20% larger over ocean than over continents, whereas the difference in effective ice crystal radius (CREI) is only about 5%.

All PDFs of effective cloud droplet radius (CREW) show a large peak around 11 μm. Additional smaller peaks around 2 μm (ISCCP and PATMOS-x) and 40 μm (ISCCP) can be explained by partly cloudy samples and by thermodynamical phase misidentification,

respectively.

Assumptions on ice crystal shape lead to additional uncertainties in retrieved effective ice crystal radius (Zhang *et al,* 2009; Zeng *et al,* 2012): ISCCP, TOVS Path-B and ATSR-GRAPE assume ice crystal aggregates, the MODIS-ST Collection 5 processing uses a mixture of ice crystal shapes and AIRS-LMD estimates the most probable shape between ice crystal aggregates and pristine hexagonal columns, the fraction of aggregates increasing with CIWP (Guignard *et al.* 2012).

The PDFs of CREI (Figure 5) fall into two categories: those using the spectral absorption at IR (8.7 μm, TOVS Path-B and AIRS-LMD) or MWIR (3.7 μm, ISCCP, PATMOS-x and MODIS-CE) and those using SWIR (2.1 μm, MODIS-ST, or 1.6 μm, ATSR-GRAPE) channels. PDFs of the first category exhibit a large peak around 32 μm with a plateau down to 20 μm, whereas PDFs of the second category exhibit a peak around 27 μm. Spectral absorption increases slightly with wavelength, so that by using shorter wavelengths one would expect to retrieve a CREI slightly deeper inside the cloud, leading to larger CREI (ice crystal size increases from cloud top to base due to aggregation processes), when the cloud statistics are similar (Zhang et al. 2010). Therefore, smaller peak values of CREI retrieved by MODIS-ST and ATSR-GRAPE may again be explained by sub-sampling, because CREI is retrieved closer to the cloud top. A smaller peak at CREI of around 18 μm produced by ISCCP can be probably explained by misidentified liquid clouds (or mixed phase clouds).

- Global cloud water path varies from 30 to 60 gm^{-2} for liquid clouds and from 60 to 120 gm^{-2} for clouds with ice tops (Figure 4). Note that these values for ice clouds include all of the cloud water in the column, some of which may actually be liquid (*cf.* Lin and Rossow 1996, Lin *et al.* 1998, Mace *et al.* 2009).
- Sub-sampling of ice clouds leads to smaller (25 gm^{-2} for semi-transparent cirrus from AIRS-LMD) or larger values (225 gm^{-2} for clouds with optical depth larger than 1 from

MODIS-ST).

PDFs of CLWP of all datasets have a peak around 70 gm^{-2}. A second peak around smaller values (1.5 gm^{-2} for PATMOS-x and ATSR-GRAPE and 8 gm^{-2} for ISCCP) may partly stem from partly cloudy samples or cloud edges.

PDFs of CIWP depend strongly on retrieval sub-sampling, with largest peaks around 5 gm^{-2} from datasets with no sub-sampling (ISCCP and PATMOS-x). Peaks move to 10 gm^{-2} and 30 gm^{-2} when excluding clouds with CEM < 0.2 (COD < 0.45) and CEM < 0.3 (COD < 0.7) respectively (AIRS-LMD and TOVS Path-B). The peak value is at to 70 gm^{-2} when excluding clouds with COD < 1 (MODIS-ST).

- The latitudinal variation of the retrieved cloud bulk microphysical properties is essentially expressed by the relative height of the peaks at small and larger values. This means that the variation (especially of CIWP) is directly linked to the difference in occurrence of optically thin and thick clouds included in each product.
- Seasonal variations .....

DIURNAL VARIATIONS

Based on ISCCP results (Cairns 1995, Rossow and Cairns 1995, Rossow and Schiffer 1999), the most noticeable features of the diurnal cycle of clouds are significant differences between the phase of low-level variations over ocean (morning maximum) and land (afternoon maximum) and between the phase of low-level and high-level cloud variations (the latter have a maximum early to late evening). These findings are complemented by analyses of IR sounder observations (exploiting the drifting NOAA satellites, Stubenrauch *et al.* 2006), which demonstrate that cirrus increase during the afternoon and gradually thicken into the nighttime. The GEWEX Cloud Assessment was mainly focused on monthly averages and longer-term variations. However, diurnal variations can affect these results. Day-night

differences and daytime sampling differences among datasets with no change in method (IR sounders and lidar) reflect random differences of a few percent (section 3.1.3 in Stubenrauch *et al.* 2012). CALIPSO seems to have a slightly smaller detection sensitivity for optically thin cirrus during the day (5 to 10% in CAHR over tropical land), linked to solar radiance noise. Day-night differences for ISCCP correspond to 5-10% in CA over land (corrected by temporal interpolation in the official ISCCP version) and approach 25% in CAHR in the tropics, the latter due primarily to the inability to adjust the height for transmissive clouds without COD information (both of these effects corrected for in the official ISCCP product).

LONGTERM VARIATIONS

Interannual variability includes natural processes which must be considered when analyzing trends. Global interannual variability lies between 0.02-0.03 in cloud amount, 2.5-3.5% in relative high-level/low-level cloud amount and around 2 K in cloud temperature. Natural interannual variability increases when considering specific regions: The most prominent feature in regional interannual variability is associated with El Niño Southern Oscillation. Monitoring longterm variations with these datasets requires consideration of many factors. Due to systematic variations of cloud properties with geographical location, time of day and season, any systematic variations in sampling of these distributions can introduce trend artifacts in the long-term record. In addition, systematic changes in instrument calibration or biases between instruments that are part of an inter-instrument data record are also problematic. These have to be carefully investigated before attributing any detected trends to climate change, which has not yet been done for any of the cloud products considered here.

CONCLUSIONS, RECOMMENDATIONS AND OUTLOOK

The GEWEX Cloud Assessment database, created by the participating teams, allowed for the first time an inter-comparison of L3 cloud products of twelve global 'state of the art'

datasets. In addition to self-assessments (Annex I of Stubenrauch *et al.* 2012) which show the maturity of the various datasets, the analyses have shown how cloud properties are perceived by instruments measuring different parts of the electromagnetic spectrum and how cloud property averages and distributions are affected by instrument choice as well as some methodological decisions. *These satellite cloud products are very valuable for climate studies or model evaluation*: Even if absolute values, especially those of high-level cloud statistics depend on instrument (or retrieval) performance to detect and/or identify thin cirrus, relative geographical and seasonal variations in the cloud properties agree very well (with only a few exceptions like deserts and snow-covered regions). Probability density functions of optical and bulk microphysical properties also agree well, when one considers retrieval sub-sampling or possible biases due to partly cloudy pixels (e.g., Zhang and Platnick 2011; Pincus *et al.* 2012) and to ice-water misidentification.

So far only ISCCP cloud properties have been tested by comparing resulting radiative fluxes to those determined from Earth Radiation Budget instruments, revealing excellent quantitative agreement (Zhang *et al.* 2004, GEWEX Assessment of Global Radiative Flux Datasets, Raschke *et al.* 2012). At present the ISCCP data record is being reprocessed. This kind of assessment should be regularly repeated, in a cycle of eight to ten years. The current GEWEX Cloud Assessment database will facilitate future activities but can be used for model evaluations, since the multiple product database can used as a cross-check on the observations. However, to obtain more robust conclusions, especially regarding dataset differences, future assessments need to be supported with funding. EUMETSAT has initiated the Cloud Retrieval Evaluation Workshop (CREW, http://www.icare.univ-lille1.fr/crew/index.php/Welcome) focusing on detailed L2 data comparisons over limited areas and time periods, and ESA included assessments of the Essential Climate Variables retrieved within the Climate Change Initiative.

ACKNOWLEDGMENTS

B. Baum, C. G. Campbell (workshop chairs), Y. Chen, A. Feofilov, A. Menzie, E. Olson, F. Parol, D. Wylie and especially other product team members)

REFERENCES

Cairns, B., 1995: Diurnal variations of cloud from ISCCP data. Atmos. Res. 37, 133-146.

Di Girolamo, L., A. Menzies, G. Zhao, and D.J. Diner, 2010: Multi-angle Imaging SpectroRadiometer cloud fraction by altitude algorithm theoretical basis, *JPL Publ., D-62358*, 19 pp.

Ferlay, N., F. Thieuleux, C. Cornet, A. B. Davis, P. Dubuisson, F. Ducos, F. Parol, J. Riedi, C. Vanbauce, 2010: Toward new inferences about cloud structures from multidirectional measurements in the oxygen A band: Middle-of-cloud pressure and cloud geometrical thickness from POLDER3/PARASOL. *J. Appl. Meteor. Clim.*, doi: 10.1175/2010JAMC2550.1

Goloub P., M. Herman, H. Chepfer, J. Riedi, G. Brogniez, P. Couvert, G. Séze, 2000: Cloud Thermodynamic Phase Classification from the POLDER Spaceborne instrument. *J. Geophys. Res.*, **105**, 14747-14759.

Guignard, A., C. J. Stubenrauch, A. J. Baran, and R. Armante, 2012: Bulk microphysical properties of semi-transparent cirrus from AIRS: a six year global climatology and statistical analysis in synergy with geometrical profiling data from CloudSat-CALIPSO. *Atmos, Chem. Phys.*, **12**, 503-525.

Heidinger, A. K., and M. J. Pavolonis, 2009: Gazing at Cirrus Clouds for 25 Years through a Split Window. Part I: Methodology. *J Appl Meteorol Clim.*, **48,** 1100-1116.

Heidinger, A. K., A. T. Evan, M. Foster, and A. Walther, 2010: A Naïve Bayesian Cloud Detection Scheme Derived from CALIPSO and Applied within PATMOS-x. *submitted JAMC.*

Holz, R., S. A. Ackerman, P. Antonelli, F. Nagle, R. O. Knuteson, M. McGill, D. L. Hlavka, and W. D. Hart, 2008: An Improvement to the High Spectral Resolution CO_2 Slicing Cloud Top Altitude Retrieval. *J. Atmos. Oceanic. Technol.*, in press.

Jin, Y., and W. B. Rossow, 1997: Detection of cirrus overlapping low-level clouds, *J. Geophys. Res.*, **102**, 1727-1737.

Liao, X., W. B. Rossow, and D. Rind, 1995: Comparison between SAGE II and ISCCP high-level clouds. Part II: Locating cloud tops. *J. Geophys. Res.*, **100**, 1137-1147.

Lin, B., and W. B. Rossow, 1996: Seasonal variation of liquid and ice water path in nonprecipitating clouds over oceans. *J. Climate*, **9**, 2890-2902.

Lin, B., Rossow, W. B., 1997: Precipitation water path and rainfall rate estimates for oceans using special sensor microwave imager and International Satellite Cloud Climatology Project data. J. Geophys. Res. 102, 9359-9374.

Mace, G. G., and S. Benson-Troth, 2002: Cloud-Layer Overlap Characteristics derived from Long-Term Cloud Radar Data, *J. Climate, 15*, 2505-2515.

Mace, G. G., Q. Zhang, M. Vaughan, R. Marchand, G. Stephens, C. Trepte, and D. Winker, 2009: A description of hydrometeor layer occurrence statistics derived from the first year of merged Cloudsat and CALIPSO data. *J. Geophys. Res.*, **114**, D00A26, doi:10.1029/2007JD009755.

Maddux, B. C., S. A. Ackerman, and S. Platnick, 2010: Viewing geometry dependencies in MODIS cloud products, *J. Atmos. Oceanic Tech.*, 27, 1519–1528.

Menzel, W. P., R. A. Frey, H. Zhang, D. P. Wylie, C. C. Moeller, R. E. Holz, B. Maddux, B. A. Baum, K. I. Strabala, and L. E. Gumley, 2008: MODIS Global Cloud-Top Pressure and Amount Estimation: Algorithm Description and Results. *J. Appl. Meteor. Climatol.*, **47**, 1175–1198.

Parol, F., J. C. Buriez, C. Vanbauce, J. Riedi, L. C. Labonnote, M. Doutriaux-Boucher, M. Vesperini, G. Sèze, P. Couvert, M. Viollier, F. M. Bréon, 2004: Capabilities of multi-angle polarization cloud measurements from satellite: POLDER results, *Adv. Space Res.*, **33**, 1080-1088.

Pincus, R., S. Platnick, S. A. Ackerman, R. S. Hemler, R. J. P. Hofmann, 2012: Reconciling simulated and observed views of clouds: MODIS, ISCCP, and the limits of instrument simulators. *J. Climate*, doi: 10.1175/JCLI-D-11-00267.1.

Platnick, S., 2000: Vertical photon transport in cloud remote sensing problems. *J. Geophys. Res.*, **105**, D18, 22,919.

Platnick, S., M. D. King, S. A. Ackerman, W. P. Menzel, B. A. Baum, J. C. Riedi, and R. A. Frey, 2003: The MODIS cloud products: Algorithms and examples from TERRA. *IEEE Trans. Geosci. Remote Sens.*, **41**, 459-473.

Poulsen

Rädel, G., C. J. Stubenrauch, R. Holz, and D. L. Mitchell, 2003: Retrieval of Effective Ice Crystal Size in the Infrared:Sensitivity Study and Global Measurements from TIROS-N Operational Vertical Sounder. *J. Geophys. Res.*, **108**, 10.1029/2002JD002801.

Raschke

Riedi, J., B. Marchant, S. Platnick, B. A. Baum, F. Thieuleux, C. Oudard, F. Parol, J.-M. Nicolas, and P. Dubuisson, 2010: Cloud thermodynamic phase inferred from merged POLDER and MODIS data. *Atmos. Chem. Phys.*, **10**, 11851-11865.

Rossow, W. B., A. W. Walker, and L. C. Garder, 1993: Comparison of ISCCP and other Cloud Amounts, *J. Climate,* **6**, 2394-2418.

Rossow, W. B., and B. Cairns, 1995: Monitoring changes of clouds. *Climatic Change*, **31**, 305-347.

Rossow, W. B., and R. A. Schiffer, 1999: Advances in understanding clouds from ISCCP. *Bull. Amer. Meteor. Soc.*, **80**, 2261-2287.

Stephens, G. L., D. G. Vane, and CloudSat Science team, 2002: The CLOUDSAT mission and the A-Train. *Bull. Amer. Meteor. Soc.*, **83**, 1771-1790.

Stubenrauch, C. J., A. Chédin, R. Armante, N. A. Scott, 1999: Clouds as seen by Infrared Sounders (3I) and Imagers (ISCCP): Part II) A New Approach for Cloud Parameter Determination in the 3I Algorithms. *J. Climate*, **12**, 2214-2223.

Stubenrauch, C. J., A. Chédin, G. Rädel, N. A. Scott, and S. Serrar, 2006: Cloud properties and their seasonal and diurnal variability from TOVS Path-B. *J. Climate*, **19**, 5531-5553.

Stubenrauch. C. J., S. Cros. A. Guignard, and N. Lamquin, 2010: A six-year global cloud climatology from the Atmospheric InfraRed Sounder aboard the AQUA Satellite: statistical analysis in synergy with CALIPSO and CloudSat. *Atmos. Chem. Phys.*, **10**, 7197-7214.

Stubenrauch, C. J., W. B. Rossow, S. Kinne and GEWEX Cloud Assessment Team, 2012: Assessment of Global Cloud Datasets from Satellites, A Project of the World Climate Research Programme Global Energy and Water Cycle Experiment (GEWEX) Radiation Panel, WCRP report, 180 pp., in revision, available at : http://climserv.ipsl.polytechnique.fr/gewexca/.

Walther, A., A. Heidinger, and M. Foster, 2011: Implementation of the Daytime Cloud Optical and Microphysical Properties Algorithm (DCOMP) in PATMOS-x. *J. Appl. Meteor. Climatol.*.

Wang, J., Rossow, W. B., Uttal, T., Rozendaal, M., 1999: Variability of cloud vertical structure during ASTEX from a combination of rawinsonde, radar, ceilometer and satellite data. *Mon. Wea. Rev.*, **127**, 2484-2502.

Wang, P.-H., R. E. Veiga, L. B. Vann, P. Minnis, and G. S. Kent, 2001: A further study of the method for estimation of SAGE II opaque cloud occurrence. *J. Geophys. Res.*, **106**, 12603-12613.

Wielicki, B. A., and L. Parker, 1992: On the determination of cloud cover from satellite sensors: The effect of sensor spatial resolution, *J. Geophys. Res.*, **97**, 12799-12823.

Winker, D. M., M. A. Vaughan, A. H. Omar, Y. Hu, K. A. Powell, Z. Liu, W. H. Hunt, and S. A. Young, 2009: Overview of the CALIPSO Mission and CALIOP Data Processing Algorithms. *J. Atmos. Oceanic Technol.*, **26**, 2310–2323.

Wylie, D. P., W. P. Menzel, H. M. Woolf, and K. I. Strabala, 1994: Four years of global cirrus cloud statistics using HIRS. *J. Climate*, **7**, 1972-1986.

Wylie, D. P., D. L. Jackson, W. P. Menzel, and J. J. Bates, 2005: Trends in Global Cloud Cover in two Decades of HIRS Observations, *J. Climate* **18**, 3021-3031.

Zeng, S., F. Parol, J. Riedi, C. Cornet, and F. Thieuleux, 2011: Examination of POLDER/PARASOL and MODIS/Aqua Cloud Fractions and Properties Representativeness, *J. Climate*, **24**, 4435-4450.

Zeng S., C. Cornet, F. Parol, J. Riedi, and F. Thieuleux, 2012 : A better understanding of cloud optical thickness derived from the passive sensors MODIS/AQUA and POLDER/PARASOL in the A-Train constellation, *Atmos. Chem. Phys. Discuss.*, **12**, 11733-11764.

Zhang *et al.* 2004

Zhang, Z., P. Yang, G. Kattawar, J. Riedi, L.-C. Labonnote, B. A. Baum, S. Platnick, and H.-L. Huang, 2009: Influence of ice particle model on satellite ice cloud retrieval: lessons learned from MODIS and POLDER cloud product comparison, *Atmos. Chem. Phys.*, 9, 7115-7129.

Zhang, Z., S. Platnick, P. Yang, A. Heidinger, and J. M. Comstock, 2010: Effect of ice particle size vertical inhomogeneity on the passive remote sensing of ice clouds, *J. Geophys. Res.*, 115, 16 pp., doi:10.1029/2010JD013835.

Zhang, Z., and S. Platnick, 2011: An assessment of differences between cloud effective particle radius for marine water clouds from three MODIS spectral bands. *J. Geophys. Res.*, 116, D20215, doi:10.1029/2011JD016216.

Sherwood *et al.* 2004
Lin *et al.* 1998

FIGURE CAPTIONS

Figure 1 : Global averages of total cloud amount (CA) and of high-level, mid-level and low-level cloud amount relative to total cloud amount (CAHR + CAMR + CALR = 1). Statistics are averaged over daytime measurements (1:30 – 3:00 PM LT, except MISR and ATSR-GRAPE at 10:30 AM LT).

Figure 2 : from left to right: Latitudinal variation relative to global annual mean of all cloud datasets, geographical map of variation relative to global annual mean of ISCCP, as well as geographical maps of the spread between maximum and minimum within six cloud datasets (ISCCP, PATMOS-x, MODIS-ST, MODIS-CE, AIRS-LMD and TOVS Path-B) of the regional variation and of the absolute value of total cloud amount (CA, top), relative high-level cloud amount (CAHR, middle) and low-level cloud amount (CALR, bottom). Statistics are averaged over daytime measurements (1:30 – 3:00 PM LT, except MISR and ATSR-GRAPE at 10:30 AM LT in the left panel).

Figure 3 : Normalized frequency distributions of cloud temperature (CT, upper panel) and of cloud pressure (CP, lower panel) in tropics (15N-15S), midlatitudes (30°-60°) and polar latitudes (60°-90°). Statistics for 2007 daytime measurements (1:30 – 3:00 PM LT).Interval limits for the definition of high-level, mid-level and low-level clouds are indicated as broken lines at 440 hPa and 680 hPa (corresponding to altitudes of about 6 km and 3 km, respectively).

Figure 4 : Global averages of cloud properties of ice clouds (I, left) and of liquid clouds (W, right): relative amount (CAR), temperature (CT), IR effective emissivity (CEM), VIS optical depth (COD), water path (CWP) and effective radius (CRE). CAWR + CAIR = 100%, except AIRS-LMD and TOVS Path-B for which the missing 35% correspond to clouds of mixed phase (230 K < CT < 260 K). CODI, CIWP and CREI are given for high-level ice clouds

instead of all ice clouds (except PATMOS-x and MODIS-ST). Statistics are averaged over daytime measurements (1:30 – 3:00 PM LT, except ATSR-GRAPE at 10:30 AM LT).

Figure 5: Normalized frequency distributions of cloud properties of ice clouds (I, left) and of liquid clouds (W, right): optical depth (COD), water path (CWP) and effective radius (CRE). Statistics are averaged over daytime measurements (1:30 – 3:00 PM LT, except ATSR-GRAPE at 10:30 AM LT).

Figure 6: Seasonal cycle of cloud properties, separately for ice clouds (left) and for liquid clouds (right) in NH midlatitudes (30N-60N) and in SH midlatitudes (30S-60S): relative fraction of clouds, optical depth, water path and effective particle radius. Statistics are averaged over daytime measurements (1:30 – 3:00 PM LT).

Table 1
Participating Datasets, type of sensors, local observation times and time period in the database

ISCCP *(Rossow and Schiffer 1999)*	multi-spectral imagers	3:00, 9:00 AM/PM	1983-2007
AVHRR Pathfinder PATMOS-x ()	multi-spectral imagers	1:30, 7:30 AM/PM	1982-2009
MODIS Science Team ()	multi-spectral imagers	1:30, 10:30 AM/PM	2001-2009
MODIS CERES Science Team ()	multi-spectral imagers	1:30, 10 :30 AM/PM	2003-2008
HIRS-NOAA ()	IR sounders	1:30, 7:30 AM/PM	1987-2006
TOVS Path-B *(Stubenrauch et al. 2006, Rädel et al. 2003)*	IR sounders	1:30, 7:30 AM/PM	1987-1994
AIRS-LMD *(Stubenrauch et al. 2010, Guignard et al. 2012)*	IR sounder	1:30 AM/PM	2003-2009
CALIPSO Science Team ()	lidar	1:30 AM/PM	2007-2008
CALIPSO-GOCCP *(Chepfer et al. 2010)*	lidar	1:30 AM/PM	2007-2008
POLDER *(Parol et al. 2004)*	multi-angle imager	1:30 PM	2006-2008
MISR ()	multi-angle imager	10:30 AM	2001-2009
ATSR-GRAPE ()	multi-angle imagers	10:30 AM	2003-2009

Table 2

Cloud Properties in GEWEX Cloud Assessment database and their range:

• Cloud amount (fractional cloud cover)	CA	(0-1)
• Cloud temperature at top	CT	(150-340 K)
• Cloud pressure at top	CP	(1013-100 hPa)
• Cloud height (above sea level)	CZ	(0-20 km)
• Cloud IR emissivity	CEM	(0-1)
• Effective Cloud amount (CA weighted by CEM)	CAE	(0-1)
• Cloud (visible) optical depth	COD	(0-400)
• Cloud water path (liquid, ice)	CLWP, CIWP	(0-3000 g/m^2)
• Cloud effective particle size (liquid, ice)	CREW, CREI	(0-200 μm)

Statistics of these variables are provided for all clouds and separately stratified by cloud top height category, defined by cloud top pressures as in ISCCP (high-level with CP < 440 hPa, mid-level with 440 hPa < CP < 680 hPa and low-level with CP > 680 hPa), and by cloud thermodynamical phase (liquid, ice), distinguished by CT (ISCCP, TOVS Path-B, AIRS-LMD), by spectral radiance differences (PATMOS-x, MODIS, ATSR-GRAPE) or by polarization signature (POLDER, CALIPSO).

Table 1: Summary of Cloud Property Retrieval Characteristics of the Datasets participating in the GEWEX Cloud Assessment

Dataset	Spatial Resolution	Cloud Detection	Variables	Retrieval Method	Ancillary Input
ISCCP	5 km, 30 km (sampled) 100 km clear sky estimation	1 VIS 1 IR window + 1 NIR over ice time – space variances	COD, CT -> CP, CZ	TB(11μm)-> CT, VIS-> COD, CT correction for COD<5	*TOVS profiles (operational)*
			Phase (WI)	ice: CT < 250 K	rad transfer+particle model
			CWP	fct(COD, phase, fixed CRE)	surf properties
			CRE	VIS/NIR LUT approach (0.6, 3.7 μm)	rad.transfer + particle model
PATMOS-x	1 km x 5 km	6 Bayesian classifiers derived from CALIPSO	CEM, CT -> CP	Optimal Estimation (11,12μm)	*NCEP reanalysis profiles (V1)*
			phase (WI)	spectral differences	MODIS snow mask
			COD, CRE	LUT approach (0.6, 3.7 μm)	rad. transfer + particle model
			CWP	CLWP=fct(CODW, CREW); CIWP=fct(CODI)	(mixed habits for ice)
HIRS-NOAA	17 km	1 IR, time – space variances	CP, CEM -> CT	CO_2 slicing for CP<650 hPa, TB(11μm)	*NCEP reanalysis profiles*
TOVSB	17 km (detection) 100 km (retrieval)	multi-spectral IR + MW clear sky estimation	CEM, CP -> CT, COD	weighted χ^2 method on CO_2 channels, COD = -2ln(1-CEM)	*TOVS profiles (TOVS Path B)*
			phase (WI)	ice: CT < 230 K	spectral surf. emissivities
			CREIH -> CIWPH	fct(CEM(8μm) CEM(11μm)), fct(CREIH,CEM(11μm))	rad.transfer + ice crystal model (aggregates)
MODIS-ST	1 km (detection, COD, CRE, CWP, phase) 5 km (CP, CT, CEM)	multi-spectral IR/NIR/VIS (16 channels) + time-space variances	CP, CEM -> CT	CO_2 slicing for CP<650 hPa, TB(11μm)	*NCEP GDAS profiles, 16day spectral surf. albedo climatology*
			phase (WI)	VIS/NIR/IR spectral differences	rad. transfer+particle model
			COD, CRE	LUT approach (0.7, 0.9, 1.2, 1.6 μm), (1.6, 2.1, 3.7 μm)	(mixed particle habits for ice)
			CWP	fct(COD,phase, CRE)	
MODIS-CE	1 km, 4 km (sampled) 32 km clear sky estimation	multi-spectral IR/NIR/VIS (5 channels similar to VIRS)	CEM, CT -> CZ, CP	IR split-window, lapse rate (7.1 K/km) +T profile	*GECS profiles*
			phase, COD, CRE	CT + LUT approach (0.6, 2.1μm), (3.8 μm)	rad. transfer+particle model
			CWP	CWP=fct(COD, CRE,phase)	(mixed habits for ice)
AIRS-LMD	14 km	spectral emissivity coherence (a posteriori)	CEM, CP -> CT, CZ, COD	weighted χ^2 method, virt. T profile for CZ, COD=-2ln(1-CEM)	*AIRS profiles (NASA, V5)*
			phase (WI)	ice: CT < 230 K	spectral surf. emissivities (AIRS/MODIS)
			CREIH, CIWPH	LUT approach on 6 spectral emissivities (9-12μm)	rad. transfer+ice crystal model (hex. columns, aggregates)
CALIPSO-ST	0.05 km x 0.34 km	lidar VIS backscatter horizontal averaging	CZ -> CT	cloud top, uppermost cloud layer (for GEWEX)	*GMAO profiles*
			phase (WI)	ice: 532 nm depolarization	
CALIPSO-GOCCP	0.48 km x 0.34 km	lidar VIS backscatter vertical averaging	CZ -> CT	cloud mean altitude,	*GMAO profiles*
				uppermost cloud layer (for GEWEX)	
POLDER	6 km (detection) 20 km (retrieval)	multi-spectral+ angle VIS/NIR threshold tests	phase (WI), COD	VIS/NIR polarization, LUT approach	rad. transfer+ particle model
			CP	O_2-A band (753,765 nm), Rayleigh (490, 565 nm)	(imom. hex. columns for ice)
MISR	1 km	multi-spectral+angle VIS/NIR	CZ	stereoscopic cloud top height	
ATSR-GRAPE	1 km (detection) 4 km (retrieval)	VIS/NIR/IR optimal estimation	COD, CP, CRE, phase -> CT	Optimal Estimation on VIS/NIR/IR (0.7,0.9,1.6,11,12 μm)	*ECMWF profiles*
			CWP	fct(COD,CRE,phase)	rad. transfer + particle model

Figures

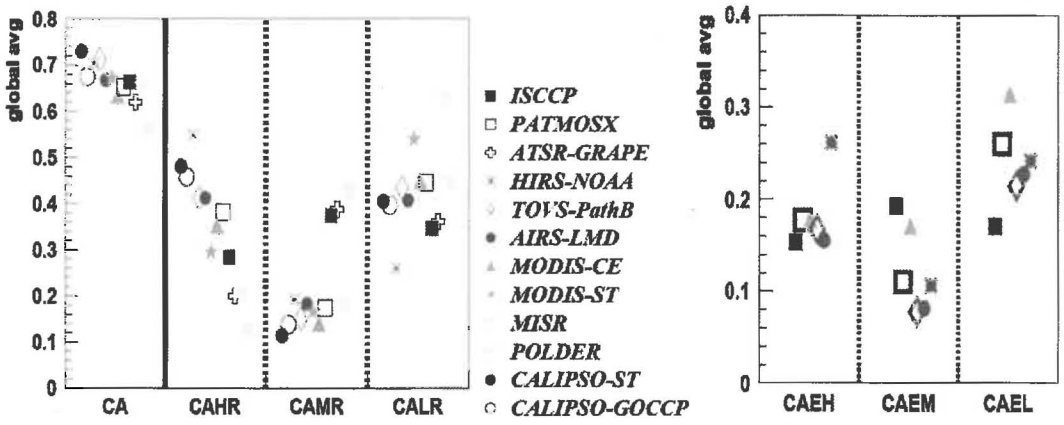

Figure 1 : Left: Global averages of total cloud amount (CA) and of high-level, mid-level and low-level cloud amount relative to total cloud amount (CAHR + CAMR + CALR = 1). Right: Global averages of effective cloud amount (cloud amount weighted by IR cloud emissivity) of high-level clouds (CAEH), of mid-level clouds (CAEM) and of low-level clouds (CAEL). Statistics are averaged over daytime measurements (1:30 – 3:00 PM LT, except MISR and ATSR-GRAPE at 10:30 AM LT).

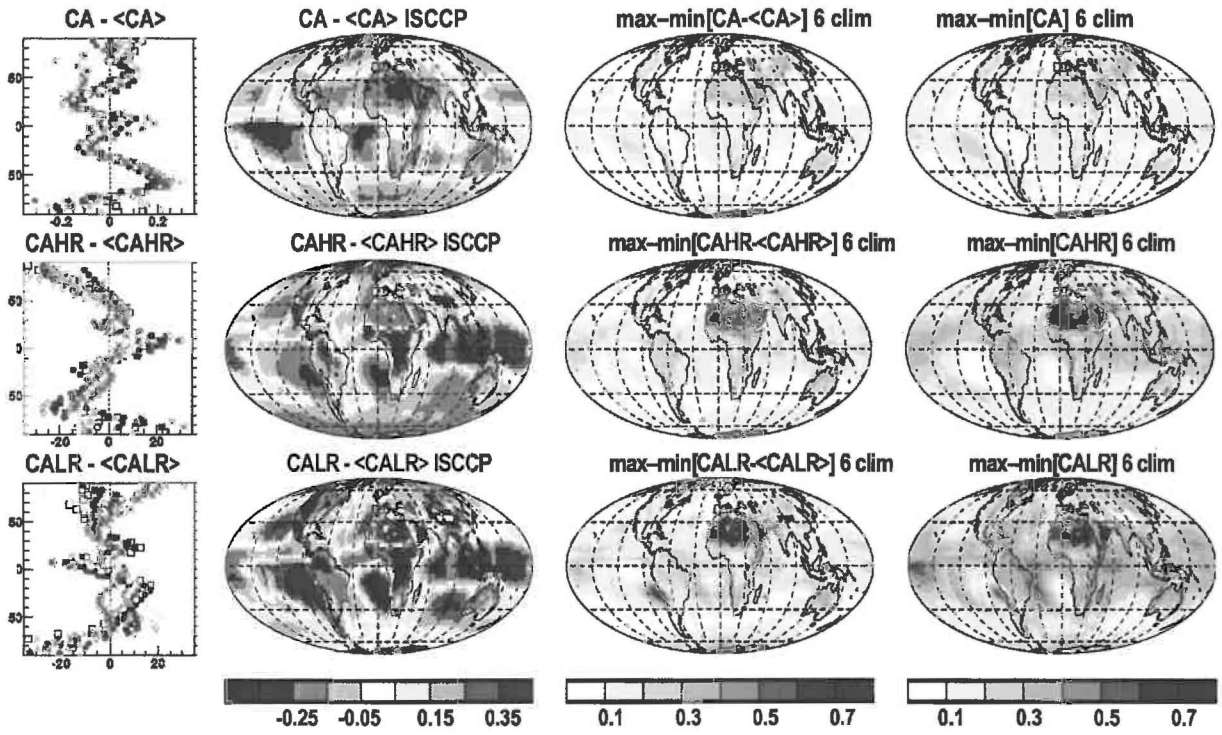

Figure 2 : from left to right: Latitudinal variation relative to global annual mean of all cloud datasets, geographical map of variation relative to global annual mean of ISCCP, as well as geographical maps of the spread between maximum and minimum within six cloud datasets (ISCCP, PATMOS-x, MODIS-ST, MODIS-CE, AIRS-LMD and TOVS Path-B) of the regional variation and of the absolute value of total cloud amount (CA, top), relative high-level cloud amount (CAHR, middle) and low-level cloud amount (CALR, bottom). Statistics are averaged over daytime measurements (1:30 – 3:00 PM LT, except MISR and ATSR-GRAPE at 10:30 AM LT in the left panel).

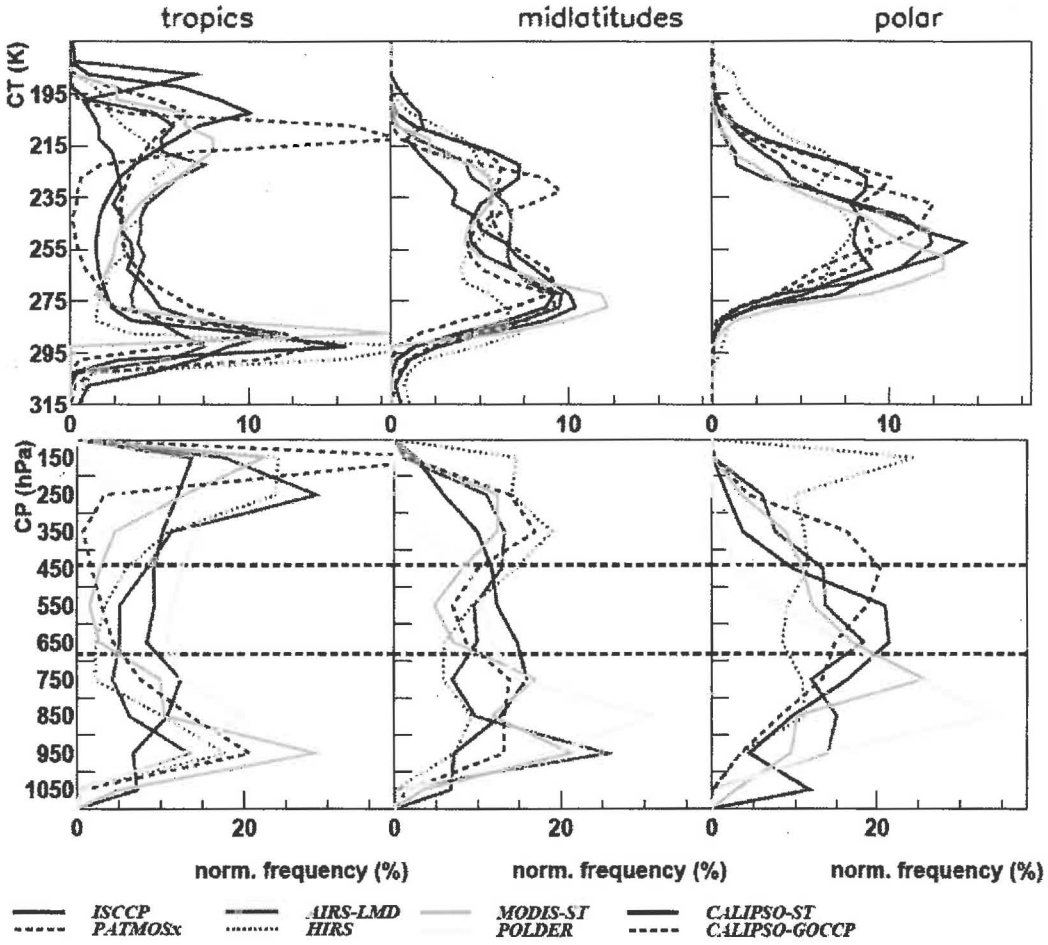

Figure 3 : Normalized frequency distributions of cloud temperature (CT, upper panel) and of cloud pressure (CP, lower panel) in tropics (15N-15S), midlatitudes (30°-60°) and polar latitudes (60°-90°). Statistics for 2007 daytime measurements (1:30 – 3:00 PM LT).Interval limits for the definition of high-level, mid-level and low-level clouds are indicated as broken lines at 440 hPa and 680 hPa (corresponding to altitudes of about 6 km and 3 km, respectively).

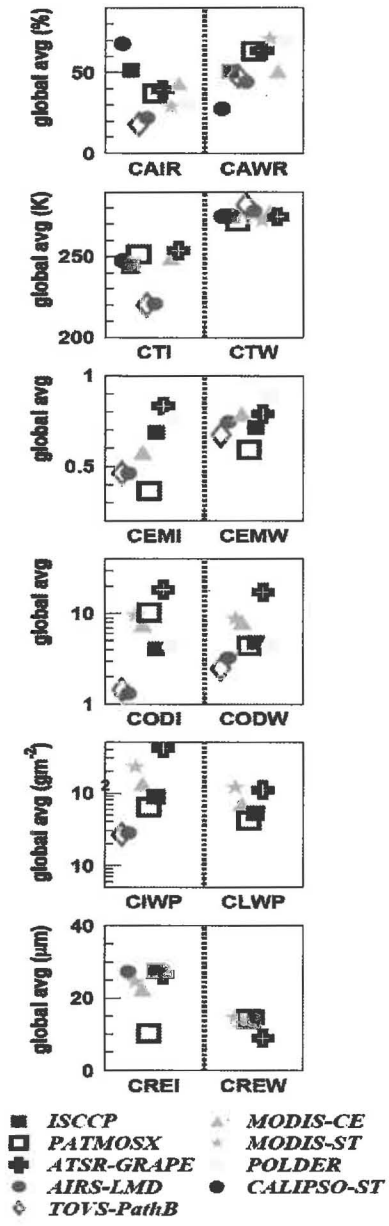

Figure 4 : Global averages of cloud properties of ice clouds (I, left) and of liquid clouds (W, right): relative amount (CAR), temperature (CT), IR effective emissivity (CEM), VIS optical depth (COD), water path (CWP) and effective radius (CRE). CAWR + CAIR = 100%, except AIRS-LMD and TOVS Path-B for which the missing 35% correspond to clouds of mixed phase (230 K < CT < 260 K). CODI, CIWP and CREI are given for high-level ice clouds instead of all ice clouds (except PATMOS-x and MODIS-ST). Statistics are averaged over daytime measurements (1:30 – 3:00 PM LT, except ATSR-GRAPE at 10:30 AM LT).

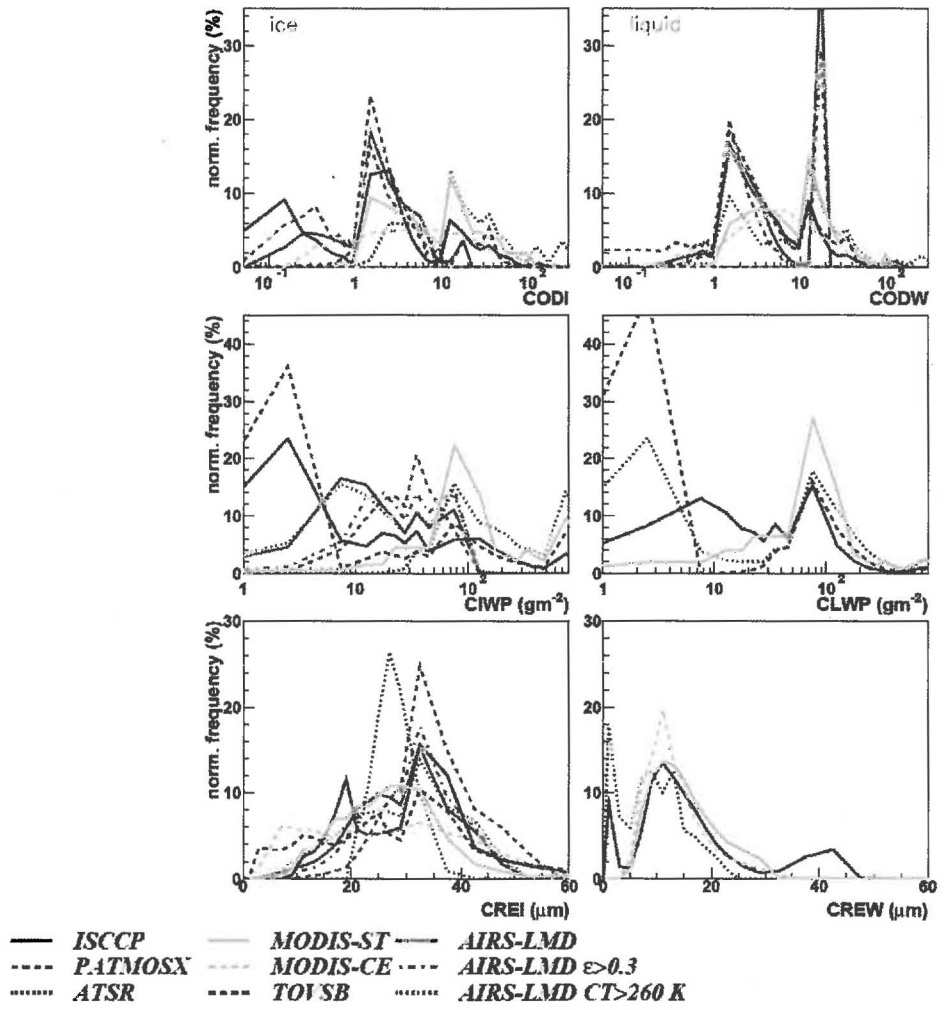

Figure 5 : Normalized frequency distributions of cloud properties of ice clouds (I, left) and of liquid clouds (W, right): optical depth (COD), water path (CWP) and effective radius (CRE). Statistics are averaged over daytime measurements (1:30 – 3:00 PM LT, except ATSR-GRAPE at 10:30 AM LT).

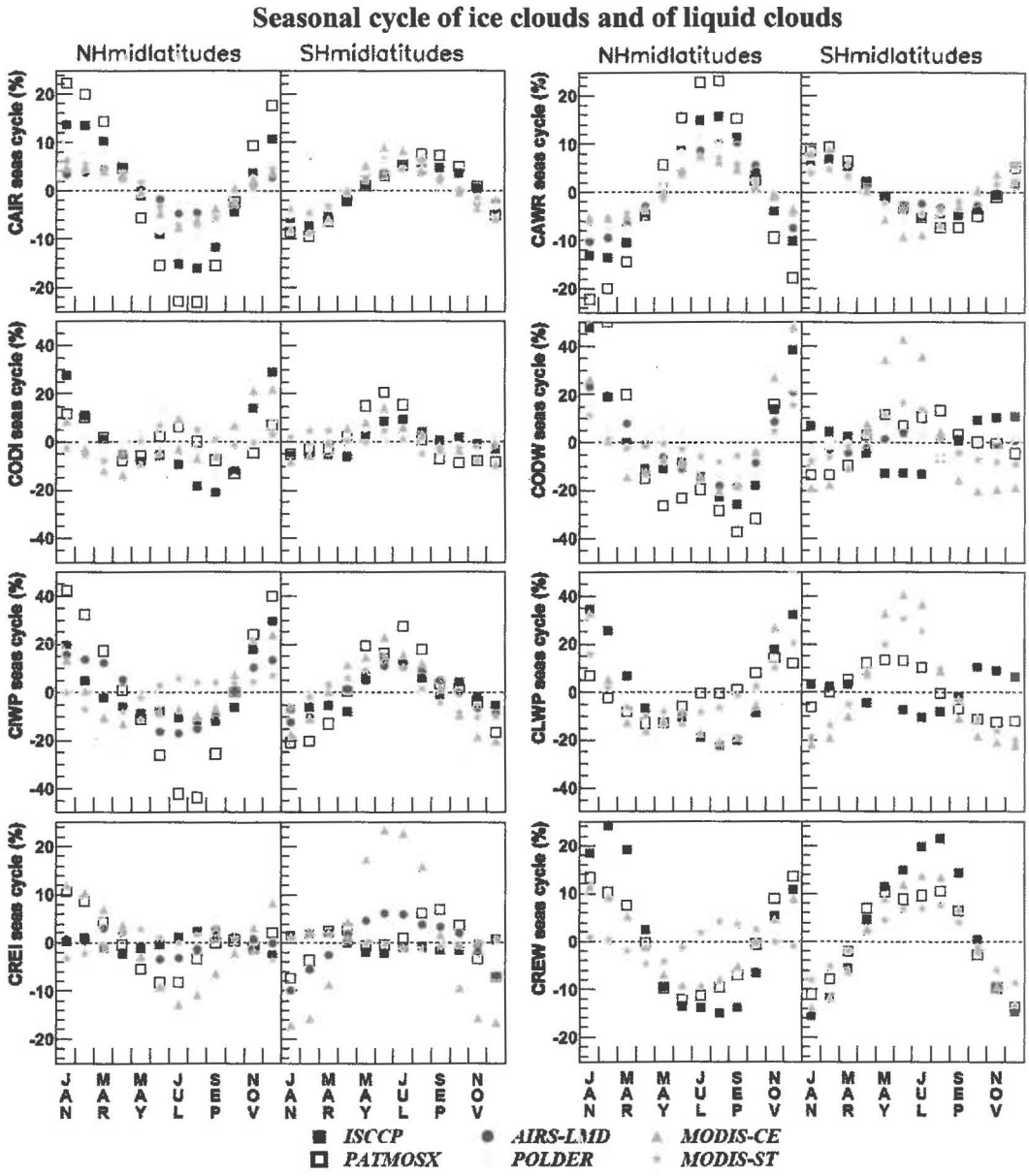

Figure 6: Seasonal cycle of cloud properties, separately for ice clouds (left) and for liquid clouds (right) in NH midlatitudes (30N-60N) and in SH midlatitudes (30S-60S): relative fraction of clouds, optical depth, water path and effective particle radius. Statistics are averaged over daytime measurements (1:30 – 3:00 PM LT).